POLITECNICO DI TORINO
Repository ISTITUZIONALE

Twofold role of columnar defects in iron based superconductors

Original
Twofold role of columnar defects in iron based superconductors / Torsello, D., Gerbaldo, R., Gozzelino, L., Laviano, F., Takahashi, A., Park, A., Pyon, S., Ichinose, A., Tamegai, T., Ghigo, G.. - In: SUPERCONDUCTOR SCIENCE & TECHNOLOGY. - ISSN 0953-2048. - ELETTRONICO. - 33:9(2020), p. 094012. [10.1088/1361-6668/aba350]

Availability:
This version is available at: 11583/2842764 since: 2020-10-28T11:52:52Z

Publisher:
IOP Publishing

Published
DOI:10.1088/1361-6668/aba350

Terms of use:

This article is made available under terms and conditions as specified in the corresponding bibliographic description in the repository

Publisher copyright

(Article begins on next page)

25 November 2026

Twofold role of columnar defects in iron based superconductors

D Torsello[1,2], R Gerbaldo[1,2], L Gozzelino[1,2], F Laviano[1,2], A Takahashi[3], A Park[3], S Pyon[3], A Ichinose[4], T Tamegai[3] and G Ghigo[1,2]

[1] Politecnico di Torino, Department of Applied Science and Technology, Torino, Italy
[2] Istituto Nazionale di Fisica Nucleare, Sez. Torino, Italy
[3] Department of Applied Physics, The University of Tokyo, Bunkyo-ku 113-8656, Tokyo, Japan
[4] Central Research Institute of Electric Power Industry, Yokosuka-shi, Kanagawa 240-0196, Japan

E-mail: daniele.torsello@polito.it

13 April 2020

Abstract. We report on the introduction of columnar defects in $Ba_{1-x}K_xFe_2As_2$ and $BaFe_2(As_{1-x}P_x)_2$ single crystals via 1.2-GeV Pb irradiation. Scanning transmission electron microscopy (STEM) analysis certifies the formation of continuous defects along the ion tracks, with a diameter of about 3 nm, and a planar density compatible with the irradiation fluence. The twofold role of such defects, i.e. as pair breakers as well as pinning centers, is investigated by a microwave technique, allowing us to determine critical temperature T_c, surface impedance and penetration depth λ_L, and by magneto-optical imaging and superconducting quantum interference device (SQUID) magnetometry to evaluate the critical current density J_c. The decrease of T_c is quite modest and, together with λ_L modifications, testifies the increase of pair-breaking scattering following irradiation. The dependence of J_c on irradiation dose and temperature is due to the pinning landscape induced by the columnar defects, and shows the existence of an optimal irradiation dose to enhance the critical current.

PACS numbers: 74.70.Xa, 74.62.En, 74.25.nn, 78.70.-g

Keywords: Iron-based superconductors, Heavy-ion irradiation, Microwave surface impedance, Critical current density, Magneto-optical imaging.

Submitted to: *Supercond. Sci. Technol.*

1. Introduction

Defects in type-II superconductors are known to play different and opposite roles: as pair breakers, they suppress the critical temperature, T_c [1, 2], and the superfluid density [3, 4], while as pinning centers they improve the critical current density, J_c, [5, 6] and the irreversibility line [7, 8]. In the last decades, this twofold role has been deeply investigated for the high-T_c cuprates [9, 10], while for relatively new superconducting materials such as the iron-based ones (IBS), a comprehensive understanding still needs to be achieved [11]. As a matter of facts, their multiband nature is responsible for further intriguing and non-trivial phenomena connected to defect-induced disorder, e.g. changes in the order parameter symmetry [12, 13, 14]. Hence, gaining for IBSs the same ability in materials engineering through defects as for the cuprates would be valuable for the sake of a better understanding of fundamental mechanisms of superconductivity [15]. One of the most efficient ways to introduce defects into superconductors is ion irradiation, allowing the creation of nanoscale defects that act as deep pinning potentials for magnetic flux lines. Indeed, this was largely demonstrated for the cuprates and also holds for IBSs. Moreover, it is noteworthy that IBSs benefit from the favourable circumstance that J_c can be enhanced by irradiation [16], while at the same time T_c is only slightly suppressed [17], namely much less than in the cuprates. This is particularly relevant, since maximizing the sustainable J_c is crucial for high-current applications of superconductivity, where also operating temperature requirements can be strict to avoid very high costs [18]. The most efficient pinning centers for superconducting vortices are defects whose morphology and dimensions match the flux-lines ones. Such defects can be generated by irradiation with swift heavy ions. In this case, defects are composed of narrow columnar tracks surrounded radially by a strained region and a distribution of pointlike defects mostly generated by secondary particles [19]. The metallic nature of IBSs causes some differences in comparison to columnar defects in the cuprates, namely different energy thresholds for the column formation and the fact that the defect core is metallic instead of insulating [20]. For this reason, thorough characterizations of IBSs in which columnar defects have been introduced is needed, as well as studies with different combinations of ions and energies in order to identify the most efficient parameters for the creation of useful defects.
In this frame, we studied the effects of defectivity generated by 1.2-GeV Pb irradiation on the properties of optimally doped $Ba_{1-x}K_xFe_2As_2$ and $BaFe_2(As_{1-x}P_x)_2$ single crystals. The defect morphology was studied by Scanning Trasmission Electron Microscopy (STEM) imaging, showing the continuity of the columnar defects along the ion tracks. The effects on the intrinsic parameters (T_c and London penetration depth) were then investigated by a microwave technique [21], while the effects on J_c and flux pinning were investigated by magneto-optical imaging [22] and magnetization measurements. The paper is structured as follows: first, all the experimental techniques employed for this study are presented in section 2, then the role of defects as scattering centers (section 3) and as pinning centers (section 4) as it emerges from experimental data is presented. Finally, these results are discussed and conclusions are drawn in section 5.

2. Techniques

2.1. Sample preparation and irradiation

Optimally doped single crystals of $Ba_{0.58}K_{0.42}Fe_2As_2$ and $BaFe_2(As_{0.67}P_{0.33})_2$ were prepared by the FeAs flux method, using as precursors FeAs, Ba, K and Ba_2As_3, Ba_2P_3, FeAs, FeP, respectively [23, 24]. The doping levels were determined by energy dispersive x-ray spectroscopy. All crystals were cleaved to be rectangular thin plates with thickness less than ~ 20 μm. This value is much smaller than the implantation depth of 1.2 GeV Pb ions in these materials as calculated with SRIM [25] and allows all the ions to go through the crystals without implanting and contributing to extra charge.
The samples were irradiated with a 1.2-GeV Pb beam at the PIAVE-ALPI facility of the INFN Legnaro Laboratories (Italy), with the beam direction parallel to the *c*-axis of the crystals. In order to minimize crystal heating under irradiation, the ion flux was kept below 1.8×10^8 cm^{-2}s^{-1}. The highest fluence achieved is 2.4×10^{12} cm^{-2}, corresponding to a dose-equivalent field (B_Φ) of 48 T.

2.2. TEM analysis

$Ba_{0.58}K_{0.42}Fe_2As_2$ samples irradiated with $B_\Phi = 4$ T were investigated by means of STEM analysis at the CRIEPI-Kanagawa Institute in Japan in both planar and cross-section configurations.
The cross-sectional STEM image reported in figure 1 shows the formation of continuous columnar tracks along the whole trajectory of the Pb ions throughout the full thickness of the sample. From the in-plane images the diameter of the columns can be estimated to be of about 3 nm. Several in-plane images taken on different areas and scales were analyzed with the image processing software ImageJ [26] to count the number of created defects and estimate their density. This density can be directly compared to

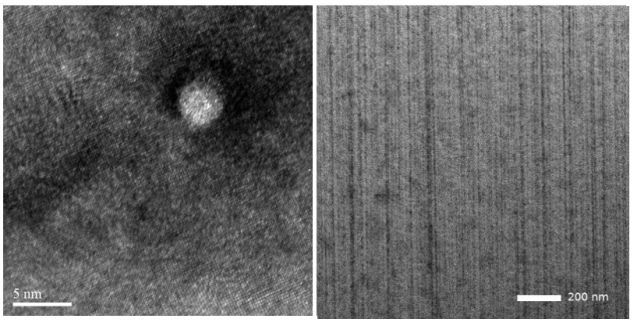


Figure 1. STEM images of a 1.2-GeV Pb irradiated $Ba_{1-x}K_xFe_2As_2$ crystal. The cross-sectional view (right) shows that straight defects are created along the ion track, while the planar view (left) shows that the columns diameter is of about 3 nm.

the irradiation fluence to evaluate the yield of the irradiation process. The number of defects was counted by blurring the STEM images to reduce noise, using the "FindMax" function of ImageJ and controlled manually on a large fraction of the analyzed images. An example for $Ba_{1-x}K_xFe_2As_2$ with $B_\Phi = 4$ T is given in figure 2. The average defects density was found to be $1.91\pm0.09\times10^{11}$ defects/cm^2, in good agreement with the irradiation fluence of the sample $1.92\pm0.09\times10^{11}$ ions/cm^2. From this analysis we can estimate a 100% yield of 1.2 GeV Pb ions in creating columnar defects. At high fluences, the possibility that more than one ion could hit the sample in the same position is relatively high, and could result in completely or partially overlapping defects.

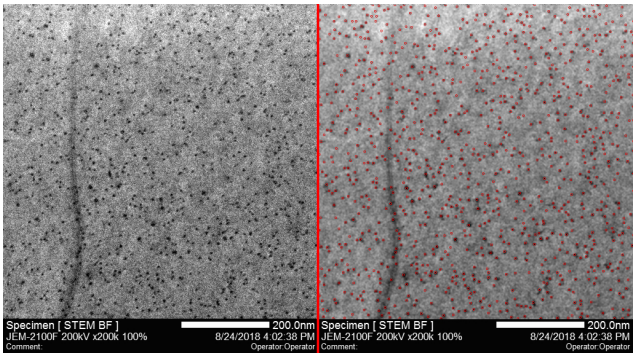


Figure 2. Left: in-plane STEM image of a 1.2-GeV Pb irradiated $Ba_{1-x}K_xFe_2As_2$ crystal. Right: same image as on the left but with the defects identified (in red) as explained in the text.

2.3. Magneto-optical imaging

The irradiated samples were preliminary characterized by means of the Magneto-Optical imaging with an Indicator Film (MOIF) technique [27, 28] that allowed us to visualize directly magnetic field distributions. The indicator film has spontaneous in-plane magnetization that is rotated out of plane by the local stray field generated by the sample. This out of plane component of the magnetization induces a rotation of the light polarization plane due to the Faraday effect. The polarization analysis in a polarization microscope is used for the visualization of the local light contrast, which is related to the local out-of-plane component of the magnetic field (B_z) in the sample. Through a nonlinear calibration, the quantitative measurement of the magnetic field is achieved. This quantity is, in turn, used to reconstruct the current density distribution (J) by an iterative algorithm [29] based on the inversion of the Biot-Savart law [30]. Exploiting the same algorithm, the in-plane magnetic field components generated by the supercurrents are also taken into account. MOIF measurements were performed on $Ba_{0.58}K_{0.42}Fe_2As_2$ and $BaFe_2(As_{0.67}P_{0.33})_2$ single crystals partially irradiated and partially kept pristine by protecting them with a suitable screen during the irradiation process. The analysis of such samples ensured that the observed modifications in the critical current can be attributed to the introduction of defects.

2.4. Surface impedance characterization

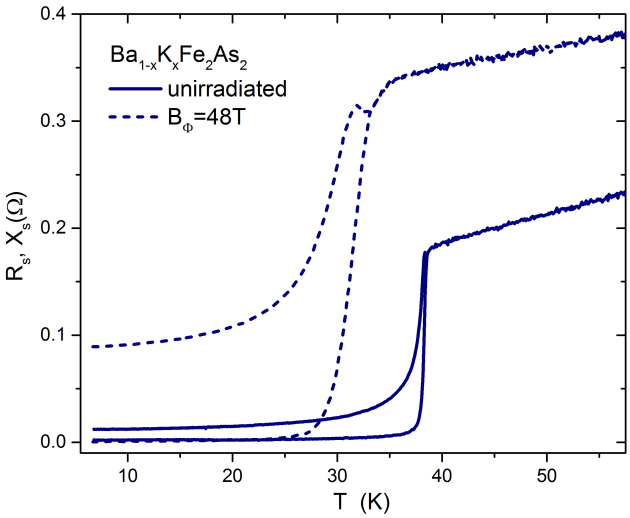


Figure 3. Real and imaginary parts of the surface impedance, $Z_s = R_s + iX_s$, for the same $Ba_{1-x}K_xFe_2As_2$ crystal, before (solid lines) and after (dashed lines) irradiation.

Microwave characterization was performed by a CoPlanar Waveguide Resonator (CPWR) technique, developed to characterize small and thin crystals [31, 32, 33]. The investigated sample was placed in the central part of the stripline of an $YBa_2Cu_3O_{7-x}$ resonator [34] and measurements of the resonance frequency and quality factor were repeated in the

same conditions, with and without the crystal. Experimental data was analyzed within a perturbative approach: the shifts of the resonant frequency and quality factor relative to no sample coupled to the resonator, after a calibration procedure, yield the London penetration depth, λ_L, and the quasiparticle conductivity σ_n[31]. The real and imaginary parts of the surface impedance (shown in figures 3 and 4 for K and P doped samples, respectively) were then obtained as:

$$Z_s = R_s + iX_s = \frac{i\omega\mu_0\lambda_L}{\sqrt{1 + i\omega\mu_0\sigma_n\lambda_L^2}}. \quad (1)$$

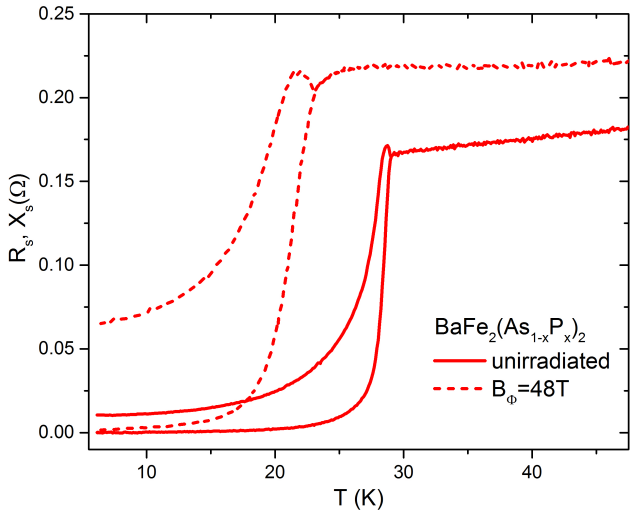


Figure 4. Real and imaginary parts of the surface impedance, $Z_s = R_s + iX_s$, for the same $BaFe_2(As_{1-x}P_x)_2$ crystal, before (solid lines) and after (dashed lines) irradiation.

2.5. Magnetization measurements

The magnetization (M) of $Ba_{1-x}K_xFe_2As_2$ crystals was measured by a superconducting quantum interference device (SQUID) magnetometer (MPMS-5XL, Quantum Design). The sample was placed in a quartz sample holder and fixed with Apiezon N grease and the applied fields were parallel to its c-axis [6]. From the magnetization data, the average bulk in-plane critical current density J_c was calculated using the extended Bean model [35] as:

$$J_c = 20\frac{\Delta M}{a(1 - b/3a)}, \quad (2)$$

where $\Delta M = M_{down}$-M_{up}, M_{up} and M_{down} are the magnetization when sweeping fields up and down respectively, and a and b ($a < b$) are the broad face dimensions of the sample.

3. Defects as scattering centers

The superconducting transition of both $Ba_{1-x}K_xFe_2As_2$ and $BaFe_2(As_{1-x}P_x)_2$ crystals, before and after irradiation, is shown in figures 3 and 4 through the temperature dependence of the complex surface impedance. Clearly, irradiation lowers T_c and broadens the transition width. The peak of $X_s(T)$ shown in figures 3 and 4 can be explained within a two-fluid model [32]. It arises because, on entering the superconducting state, the initial reduction in normal electrons is not immediately compensated, in terms of screening of the microwave field, by the increase of the superconducting current [36]. The peak is wider but not higher after irradiation, whereas in the case of 250 MeV Au ion irradiation the peak maximum value was strongly enhanced with respect to the value at T_c [32].

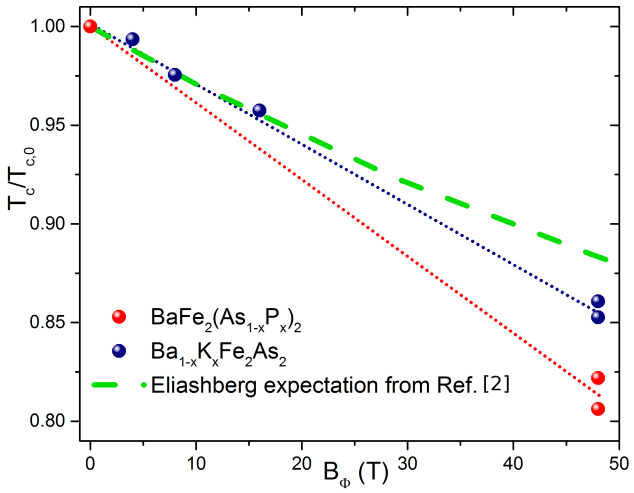


Figure 5. Critical temperature variation with respect to the pristine value $T_{c,0}$ due to irradiation with 1.2-GeV Pb ions, as a function of the dose equivalent field, for both the K-doped (navy simbols) and the P-doped (red symbols) crystals. In green dashed lines the expected decrease of critical temperature due to interband scattering (as calculated using the Eliashberg equations in Ref. [2]) is reported.

The critical temperature suppression due to irradiation is shown in figure 5 for $Ba_{1-x}K_xFe_2As_2$ in blue and $BaFe_2(As_{1-x}P_x)_2$ in red. The P doped material seems to be slightly more affected by irradiation than the K doped one. This might be related to the fact that K substitution acts on the spacer layers, whereas P substitution directly affects the FeAs layers making the system slightly more fragile [37]. In order to qualitatively show that T_c degradation is ascribable to interband scattering due to defects, we compare the experimental critical temperature suppression rates to the expected one in the case of similar defects in $Ba_{1-x}K_xFe_2As_2$ (dashed green line in

figure 5) discussed in Ref. [2]. The calculations (carried out within an Eliashberg approach) refer to irradiation with 250 MeV Au ions that produce discontinuous correlated tracks [38] instead of continuous columnar ones as in the case of 1.2 GeV Pb ions. Despite this difference, the overall typology of defect is comparable [39] and results in a similar T_c suppression rate [2, 40]. Due to these similarities and differences, we can interpret the reasonable agreement between the experimental data and the calculations (not optimized for the present case) as a confirmation of the fact that the T_c degradation is due to pair-breaking scattering induced by the defects introduced by irradiation (both columnar core and surrounding pointlike).

Figure 6 shows the London penetration depth as

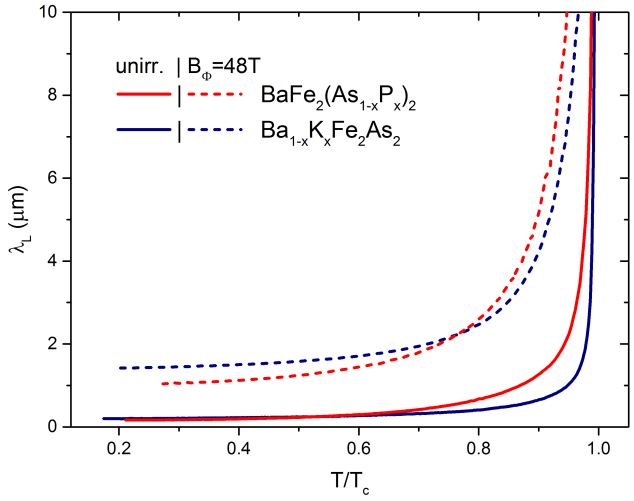


Figure 6. London penetration depth of the investigated crystals, before (solid lines) and after (dashed lines) irradiation, as a function of the reduced temperature, T/T_c for both the K-doped (navy) and the P-doped (red) crystals.

a function of the reduced temperature, for the two compounds, before and after irradiation. The shift of the curves after irradiation is similar for the two systems. For both of them, a noticeable increase of the low temperature value of λ_L was observed, similar to that observed after irradiation of Ba122 systems with 250-MeV Au ions [2] and 3.5-MeV protons [14], also independently of the experimental approach used [41]. Notably, also this kind of modifcations can be attributed to the effects of pair-breaking interband scattering [2, 4].

4. Defects as pinning centers

The critical current density increase due to the contribution of defects as pinning centers can be easily visualized by the MOIF technique [42]. Figure 7 shows the spatial distributions of fields and currents in samples of

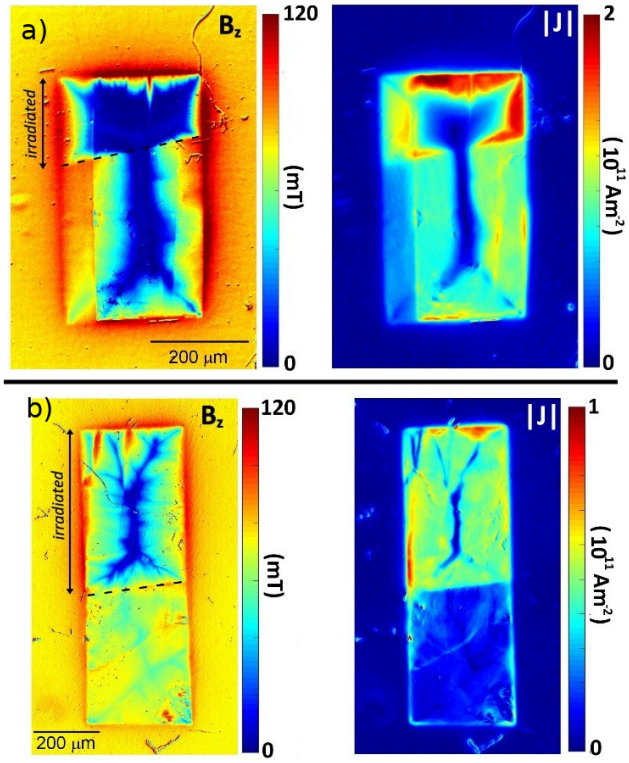


Figure 7. Quantitative MOIF (magnetic field and current density distribution) of partly irradiated $Ba_{1-x}K_xFe_2As_2$ (a) and $BaFe_2(As_{1-x}P_x)_2$ (b) single crystals (B_Φ=0.1 T). The images are taken at T = 8 K and applied magnetic field is 73 mT.

$Ba_{1-x}K_xFe_2As_2$ and $BaFe_2(As_{1-x}P_x)_2$ at low temperature (T= 8 K) and applied field ($\mu_0 H$=73 mT) for an irradiation fluence corresponding to a dose-equivalent field B_Φ=0.1 T.

The images of the as-grown parts show that doping in crystals is rather uniform and the inhomogeneity of the current density distribution is due to macroscopic defects like cracks or small steps (different thickness).

The irradiated parts of the crystals are clearly visible both in the magnetic field and in the current density distribution: the irradiation enhanced the critical current density and hence the vortex penetration is retarded. The crystals were irradiated together, therefore the different enhancement of the critical current density, between irradiated and as-grown parts (a factor of about 2 for $Ba_{1-x}K_xFe_2As_2$ and of about 4 in $BaFe_2(As_{1-x}P_x)_2$), can be related either to the intrinsic microscopic differences in superconducting properties between the two compositions or to the as-grown pinning landscape.

Further details of the in-field critical current density and the pinning anisotropy studied by MOIF in these samples will be reported in a separated work.

The dependence of the critical current on the irradiation dose, applied field, and temperature was studied

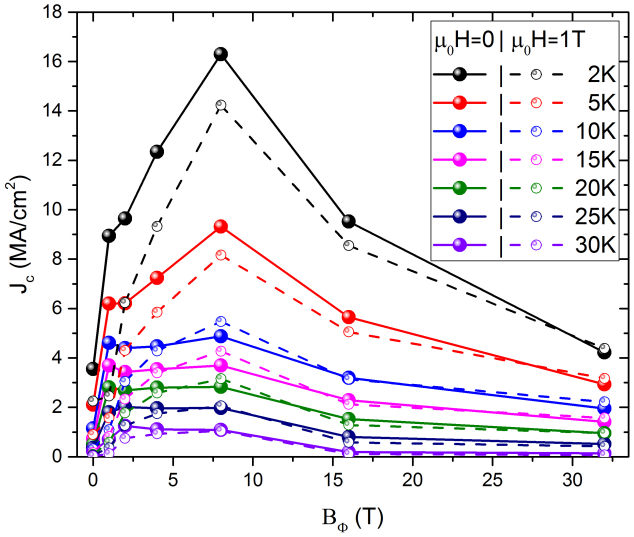


Figure 8. Critical current density of $Ba_{1-x}K_xFe_2As_2$ samples as a function of irradiation dose-equivalent field for different temperatures at zero field and for an applied field of 1 T parallel to the defects axis.

by magnetization measurements, as explained in the previous section. The dependence on these three parameters is summarized in figure 8 for $Ba_{1-x}K_xFe_2As_2$ samples, and several aspects can be discussed starting from it.

First of all, it is evident that the introduction of columnar defects (increase of B_Φ) enhances the critical current through vortex pinning: at low temperature and zero applied field the maximum increase is almost five-fold, starting from a reasonably large value of J_c=3.5 MA/cm^2. However, this increment is not monotonic, as will be discussed below. Moreover, it should be noted that the pinning landscape responsible for the increase of the critical current density is given by both the narrow columns and the broader distribution of pointlike defects combined [43, 44].

The dependence of J_c on temperature (at fixed applied field and irradiation dose) is, as expected, always monotonic. Conversely, at certain fixed temperatures and fluences (*e.g.* B_Φ=8 T, T=10 K), the value of J_c at self-field is lower than at 1 T. This is due to the curvature of vortices at fields lower than the self field [11].

In addition, for all temperatures and values of applied field, the critical current has a maximum at the irradiation dose B_Φ=8 T, this feature is particularly evident at low temperature. This could be interpreted as follows: at low fluences J_c is highly enhanced by efficient vortex pinning from columnar defects. However, at high doses the defects are closer and closer together (possibly even overlapping), resulting in a more uniform pinning landscape where the pinning potential is not as deep and steep, and the vortices have a higher mobility from one pinning site to another. This is also in agreement with the observation that, as the energy of the ions increases, the diameter of the columnar defects becomes smaller (which is confirmed in TEM images [38]) and the observed peak of J_c as a function of B_Φ shifts to higher values [40]. Namely, the B_Φ value at which J_c peaks might be directly related to the ratio of columnar defect diameter to average distance of defects.

5. Discussion and conclusions

In this work, we have highlighted the double role of columnar defects introduced in IBSs via high energy heavy ion (1.2 GeV Pb) irradiation as pair breaking scattering centers and as vortex pinning centers. STEM analysis confirmed the production of continuous columnar defects with a diameter of $\sim$ 3 nm. The density of such defects is equal to the irradiation fluence and confirms a 100% yield in the defect production.

CPWR measurements of the critical temperature, surface impedance and London penetration depth demonstrate the enhancement of pair breaking scattering events following irradiation. However, the degradation of T_c is quite modest when compared to the cuprate family (transport measurement on $YBa_2Cu_3O_{7-x}$ thin films irradiated in the same conditions, during the same irradiation run, show a decrease of T_c $\sim$ 5 K for B_Φ $\sim$ 8 T with respect of only 1 K decrease for $Ba_{1-x}K_xFe_2As_2$). The modifications of Z_s and λ_L in the K-doped and P-doped $BaFe_2As_2$ systems are comparable although there are some small differences that could be related to the different chemical substitutions that intervene in the spacing or in FeAs superconducting layers, respectively.

MOIF and magnetization measurements allowed us to discuss the role of columnar defects as pinning centers. MOIF images confirmed the homogeneity of samples properties and of defects distribution, and allowed us to attribute the observed J_c modifications to the introduction of columnar defects. The dependence of J_c on irradiation dose and temperature was studied through magnetization measurements, showing the existence of an optimal irradiation dose (B_Φ $\sim$ 8 T) to enhance the critical current. The value of this optimal dose might depend on the specific ion-energy combination employed for the irradiation that results in a specific size of the introduced columnar defects, and therefore in the pinning landscape.

This set of information can lead to the choice of protocols for the optimization of the superconducting properties of iron-based superconducting coated conductors or tapes, that have already risen a relevant technolgical

interest in the field of power transport and generation of strong magnetic fields.

Acknowledgments

This work was partially supported by the Italian Ministry of Education, University and Research (Project PRIN HIBiSCUS, Grant No. 201785KWLE) and by a Grant-in-Aid for Scientific Research (A) (Grant No. 17H01141) from the Japan Society for the Promotion of Science (JSPS). The irradiations were performed in the framework of the INFN-Politecnico di Torino M.E.S.H. Research Agreement.

References

[1] Bang Y, Choi H Y and Won H 2009 *Phys. Rev. B* **79**(5) 054529
[2] Ghigo G, Ummarino G A, Gozzelino L, Gerbaldo R, Laviano F, Torsello D and Tamegai T 2017 *Sci. Rep.* **7** 13029
[3] Efremov D V, Korshunov M M, Dolgov O V, Golubov A A and Hirschfeld P J 2011 *Phys. Rev. B* **84** 180512(R)
[4] Torsello D, Ummarino G A, Gerbaldo R, Gozzelino L and Ghigo G 2019 *J. Supercond. Nov. Magn.* 1
[5] Civale L, Marwick A D, Worthington T K, Kirk M A, Thompson J R, Krusin-Elbaum L, Sun Y, Clem J R and Holtzberg F 1991 *Phys. Rev. Lett.* **67**(5) 648
[6] Taen T, Ohtake F, Pyon S, Tamegai T and Kitamura H 2015 *Supercond. Sci. Technol.* **28** 085003
[7] Hardy V, Provost J, Groult D, Hervieu M, Raveau B, Durčok S, Pollert E, Frison J, Chaminade J and Pouchard M 1992 *Physica C* **191** 85
[8] Kwok W K, Welp U, Glatz A, Koshelev A E, Kihlstrom K J and Crabtree G W 2016 *Rep. Prog. Phys.* **79** 116501
[9] Hardy V, Groult D, Provost J, Hervieu M, Raveau B and Bouffard S 1991 *Physica C* **178** 255
[10] Zhu Y, Cai Z X, Budhani R C, Suenaga M and Welch D O 1993 *Phys. Rev. B* **48**(9) 6436
[11] Tamegai T, Taen T, Yagyuda H, Tsuchiya Y, Mohan S, Taniguchi T, Nakajima Y, Okayasu S, Sasase M, Kitamura H, Murakami T, Kambara T and Kanai Y 2012 *Supercond. Sci. Technol.* **25** 084008
[12] Kontani H and Onari S 2010 *Phys. Rev. Lett.* **104**(15) 157001
[13] Schilling M B, Baumgartner A, Gorshunov B, Zhukova E S, Dravin V A, Mitsen K V, Efremov D V, Dolgov O V, Iida K, Dressel M and Zapf S 2016 *Phys. Rev. B* **93** 174515
[14] Ghigo G, Torsello D, Ummarino G A, Gozzelino L, Tanatar M A, Prozorov R and Canfield P C 2018 *Phys. Rev. Lett.* **121**(10) 107001
[15] Wang Y, Kreisel A, Hirschfeld P J and Mishra V 2013 *Phys. Rev. B* **87** 094504
[16] Takahashi A, Pyon S, Okayasu S, Ishida S, Iyo A, Eisaki H, Imai M, Abe H, Terashima T and Tamegai T 2019 *J. Phys.: Conf. Ser.* **1293** 012013
[17] Sylva G, Bellingeri E, Ferdeghini C, Martinelli A, Pallecchi I, Pellegrino L, Putti M, Ghigo G, Gozzelino L, Torsello D, Grimaldi G, Leo A, Nigro A and Braccini V 2018 *Supercond. Sci. Technol.* **31** 054001
[18] Putti M, Pallecchi I, Bellingeri E, Cimberle M R, Tropeano M, Ferdeghini C, Palenzona A, Tarantini C, Yamamoto A, Jiang J, Jaroszynski J, Kametani F, Abraimov D, Polyanskii A, Weiss J D, Hellstrom E E, Gurevich A, Larbalestier D C, Jin R, Sales B C, Sefat A S, McGuire M A, Mandrus D, Cheng P, Jia Y, Wen H H, Lee S and Eom C B 2010 *Supercond. Sci. Technol.* **23** 034003
[19] Biswal R, John J, Behera D, Mallick P, Kumar S, Kanjilal D, Mohanty T, Raychaudhuri P and Mishra N C 2008 *Supercond. Sci. Technol.* **21** 085016
[20] Massee F, Sprau P O, Wang Y L, Davis J C S, Ghigo G, Gu G D and Kwok W K 2015 *Sci. Adv.* **1**(4) e1500033
[21] Torsello D, Cho K, Joshi K R, Ghimire S, Ummarino G A, Nusran N M, Tanatar M A, Meier W R, Xu M, Bud'ko S L, Canfield P C, Ghigo G and Prozorov R 2019 *Phys. Rev. B* **100**(9) 094513
[22] Laviano F, Botta D, Chiodoni A, Gerbaldo R, Ghigo G, Gozzelino L and Mezzetti E 2003 *Phys. Rev. B* **68**(1) 014507
[23] Kihou K, Saito T, Ishida S, Nakajima M, Tomioka Y, Fukazawa H, Kohori Y, Ito T, Uchida S i, Iyo A, Lee C H and Eisaki H 2010 *J. Phys. Soc. Jpn.* **79** 124713
[24] Nakajima M, Uchida S i, Kihou K, Lee C H, Iyo A and Eisaki H 2012 *J. Phys. Soc. Jpn.* **81** 104710
[25] Ziegler J F, Ziegler M and Biersack J 2010 *Nucl. Instrum. Meth. B* **268** 1818
[26] Schneider C A, Rasband W S and Eliceiri K W 2012 *Nature methods* **9** 671
[27] Dorosinskii L, Indenbom M, Nikitenko V, Ossip'yan Y A, Polyanskii A and Vlasko-Vlasov V 1992 *Physica C* **203** 149
[28] Helseth L E, Solovyev A G, Hansen R W, Il'yashenko E I, Baziljevich M and Johansen T H 2002 *Phys. Rev. B* **66**(6) 064405
[29] Laviano F, Botta D, Chiodoni A, Gerbaldo R, Ghigo G, Gozzelino L, Zannella S and Mezzetti E 2003 *Superconductor Science and Technology* **16** 71
[30] Jooss C, Albrecht J, Kuhn H, Leonhardt S and Kronmller H 2002 *Rep. Prog. Phys.* **65** 651
[31] Ghigo G, Ummarino G A, Gozzelino L and Tamegai T 2017 *Phys. Rev. B* **96** 014501
[32] Ghigo G, Torsello D, Gerbaldo R, Gozzelino L, Laviano F and Tamegai T 2018 *Supercond. Sci. Technol.* **31** 034006
[33] Ghigo G, Torsello D, Gozzelino L, Tamegai T, Veshchunov I S, Pyon S, Jiao W, Cao G H, Grebenchuk S Y, Golovchanskiy I A, Stolyarov V S and Roditchev D 2019 *Phys. Rev. Research* **1**(3) 033110
[34] Ghigo G, Laviano F, Gerbaldo R and Gozzelino L 2012 *Supercond. Sci. Technol.* **25** 115007
[35] Bean C P 1964 *Rev. Mod. Phys.* **36**(1) 31
[36] Ormeno R J, Hein M A, Barraclough T L, Sibley A, Gough C E, Mao Z Q, Nishizaki S and Maeno Y 2006 *Phys. Rev. B* **74**(9) 092504
[37] Torsello D, Ummarino G A, Gozzelino L, Tamegai T and Ghigo G 2019 *Phys. Rev. B* **99**(13) 134518
[38] Nakajima Y, Tsuchiya Y, Taen T, Tamegai T, Okayasu S and Sasase M 2009 *Phys. Rev. B* **80** 012510
[39] Ito N, Pyon S, Kambara T, Yoshida A, Okayasu S, Ichinose A and Tamegai T 2018 *J. Phys.: Conf. Ser.* **1054** 012020
[40] Takahashi A 2019 Thesis
[41] Kim J, Haberkorn N, Graf M J, Usov I, Ronning F, Civale L, Nazaretski E, Chen G F, Yu W, Thompson J D and Movshovich R 2012 *Phys. Rev. B* **86**(14) 144509
[42] Laviano F, Gerbaldo R, Ghigo G, Gozzelino L, Mikitik G P, Taen T and Tamegai T 2014 *Supercond. Sci. Technol.* **27** 044014
[43] Sadovskyy I, Jia Y, Leroux M, Kwon J, Hu H, Fang L, Chaparro C, Zhu S, Welp U, Zuo J., Zhang Y, Nakasaki R, Selvamanickam V, Crabtree G, Koshelev A, Glatz A and Kwok W 2016 *Adv. Mater.* **28** 4593
[44] Jia Y, LeRoux M, Miller D, Wen J, Kwok W, Welp U, Rupich M, Li X, Sathyamurthy S, Fleshler S, Malozemoff A, Kayani A, Ayala-Valenzuela O and Civale L 2013 *Appl. Phys. Lett.* **103** 122601